Semiconducting Nanostructures

Deutsche Ausgabe: DOI: 10.1002/ange.201501364
Internationale Ausgabe: DOI: 10.1002/anie.201501364

Unambiguous Diagnosis of Photoinduced Charge Carrier Signatures in a Stoichiometrically Controlled Semiconducting Polymer-Wrapped Carbon Nanotube Assembly**

*Jean-Hubert Olivier, Jaehong Park, Pravas Deria, Jeff Rawson, Yusong Bai, Amar S. Kumbhar, and Michael J. Therien**

Dedicated to Professor Harry B. Gray on the occasion of his 80th birthday

Abstract: *Single-walled carbon nanotube (SWNT)-based nanohybrid compositions based on (6,5) chirality-enriched SWNTs ([(6,5) SWNTs]) and a chiral n-type polymer (S-PBN(b)-Ph$_4$PDI) that exploits a perylenediimide (PDI)-containing repeat unit are reported; S-PBN(b)-Ph$_4$PDI-[(6,5) SWNT] superstructures feature a PDI electron acceptor unit positioned at 3 nm intervals along the nanotube surface, thus controlling rigorously SWNT–electron acceptor stoichiometry and organization. Potentiometric studies and redox-titration experiments determine driving forces for photoinduced charge separation (CS) and thermal charge recombination (CR) reactions, as well as spectroscopic signatures of SWNT hole polaron and PDI radical anion (PDI$^{-\bullet}$) states. Time-resolved pump–probe spectroscopic studies demonstrate that S-PBN(b)-Ph$_4$PDI-[(6,5) SWNT] electronic excitation generates PDI$^{-\bullet}$ via a photoinduced CS reaction ($\tau_{CS} \approx 0.4$ ps, $\Phi_{CS} \approx 0.97$). These experiments highlight the concomitant rise and decay of transient absorption spectroscopic signatures characteristic of the SWNT hole polaron and PDI$^{-\bullet}$ states. Multiwavelength global analysis of these data provide two charge-recombination time constants ($\tau_{CR} \approx 31.8$ and 250 ps) that likely reflect CR dynamics involving both an intimately associated SWNT hole polaron and PDI$^{-\bullet}$ charge-separated state, and a related charge-separated state involving PDI$^{-\bullet}$ and a hole polaron site produced via hole migration along the SWNT backbone that occurs over this timescale.*

The unique optical[1] and electrical[2] properties of semiconducting single-walled carbon nanotubes (SWNTs) fuel interest in the development of SWNT-based nanohybrid materials for energy conversion and optoelectronic devices.[3] Exploitation of SWNTs as light-harvesting and charge-transport materials in solar cells, for example, would be greatly facilitated by the evolution of nanoscale assemblies that provide facile generation of electron–hole pairs at organized nanotube–soft-matter interfaces. In contrast to covalent sidewall functionalization that disrupts fundamental nanotube electronic properties, use of electron-rich[4] or electron-deficient[5] chromophoric surfactant molecules as semiconducting SWNT-solubilizing agents provides nanostructures in which photoexcitation may trigger charge separation. While these pioneering studies define important proofs-of-principle that photoinduced charge-transfer reactions can take place at SWNT/organic chromophore interfaces, many challenges remain. These include the inability to: 1) control the stoichiometry of electron (hole) acceptors at the nanotube interface; 2) regulate the hole (electron) polaron density generated per nanotube unit length for a defined set of irradiation conditions; 3) structure electrooptically functional SWNT-based nanohybrids over macroscopic length scales; and 4) engineer nanotube–soft-matter assemblies in which photoinduced charge separation (CS) and thermal charge recombination (CR) dynamics can be rigorously elucidated and ultimately modulated. This latter challenge is of critical importance, as optimization of light-driven electron–hole pair generation, separation, and persistence requires fundamental new insights into the design of hybrid nanomaterial electronic structures.

Pump–probe transient optical spectroscopic data that examine photoinduced CS and thermal CR dynamics of nanotube-containing charge-transfer assemblies have typically been characterized by multiple bleaching bands that broadly span the Vis and NIR spectral windows, as standard SWNT samples feature heterogeneous distributions of nano-

[*] Dr. J.-H. Olivier,[+] Dr. J. Park,[+] Dr. P. Deria, Dr. J. Rawson, Y. Bai, Prof. M. J. Therien
Department of Chemistry, Duke University
French Family Science Center
124 Science Drive, Durham, NC 27708 (USA)
E-mail: michael.therien@duke.edu
Homepage: http://www.chem.duke.edu/~mt83/
Dr. J. Park[+]
Department of Chemistry, University of Pennsylvania
231 South 34th Street, Philadelphia, PA 19104-6323 (USA)
Dr. A. S. Kumbhar
Chapel Hill Analytical & Nanofabrication Laboratory
University of North Carolina at Chapel Hill
243 Chapman Hall, NC 27599 (USA)
[+] These authors contributed equally to this work.

[**] This work was funded by the Division of Chemical Sciences, Geosciences, and Biosciences, Office of Basic Energy Sciences, of the U.S. Department of Energy through Grant DE-SC0001517. Infrastrucutral support provided by NSF NSEC DMR 08-32802 is gratefully acknowledged.

Supporting information for this article is available on the WWW under http://dx.doi.org/10.1002/anie.201501364.

tube chiralities and lengths: the spectral congestion characteristic of such samples makes difficult the identification of the electronic signatures that distinguish electron-transfer (ET) reactants and products (that is, chromophore/SWNT electronically excited states, organic cation/anion radical species, and nanotube hole/electron polaron states), and corresponding analyses of charge separation, charge migration, and charge recombination dynamics. Herein, we delineate SWNT-based nanohybrid compositions based on (6,5) chirality-enriched SWNTs ([(6,5) SWNTs], obtained in greater than 85% purity through a combination of linear and nonlinear density gradient ultracentrifugation; see the Supporting Information),[6] and a novel chiral n-type polymer (*S*-PBN(b)-Ph_4PDI) that features a perylenediimide (PDI)-containing repeat unit (Scheme 1; Supporting Information).

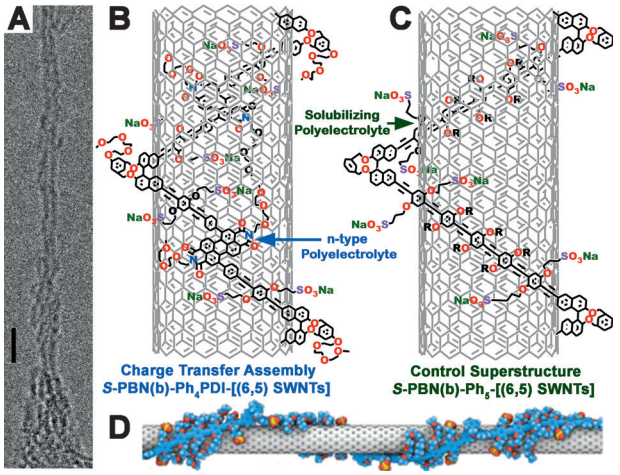

Scheme 1. A) TEM images of the *S*-PBN(b)-Ph_4PDI-[(6,5) SWNT] charge-transfer assembly obtained from aqueous suspension (scale bar: 5 nm); B) depiction of the *S*-PBN(b)-Ph_4PDI-[(6,5) SWNT] superstructure, and C) a corresponding depiction of a *S*-PBN(b)-Ph_5-[(6,5) SWNT], which defines a control-polymer–SWNT superstructure for transient pump–probe studies that interrogate photoinduced charge separation and thermal charge recombination dynamics in S-PBN(b)-Ph_4PDI-[(6,5) SWNTs]. D) Depiction of a chiral [arylene]ethynylene polymer-wrapped SWNT.

S-PBN(b)-Ph_4PDI helically wraps the nanotube surface in an exclusive left-handed[7] manner (*S*-PBN(b)-Ph_4PDI-[(6,5) SWNTs], Scheme 1). In contrast to polyfluorene-based polymers that interact with SWNTs to form nanomaterials that feature an ill-defined interfacial arrangement, *S*-PBN(b)-Ph_4PDI is a member of a class of highly charged [arylene]-ethynylene polymers that have previously been established to exfoliate, individualize, and single-chain wrap the nanotube surface with periodic and constant morphology.[7] Extensive AFM and TEM data demonstrate a helix pitch length of 9 ± 2 nm (Supporting Information, Figure S5, S6) for *S*-PBN(b)-Ph_4PDI-[(6,5) SWNTs], and that these semiconducting polymer-SWNT superstructures are robust in a wide range of aqueous and organic solvents.[7,8] Note that the single-chain polymer-wrapping mechanism characteristic of these superstructures solubilizes the nanotube at a minimal polymer/SWNT molar ratio, and provides a facile means to organize functional organic moieties at predefined intervals along the SWNT surface. Closely related assemblies have been utilized to provide new insights into SWNT electronically excited states,[1a,6a] interrogate SWNT biexciton dynamics,[9] and characterize SWNT hole polaron states.[10] *S*-PBN(b)-Ph_4PDI-[(6,5) SWNTs] (Scheme 1), which feature the widely utilized PDI unit[11] positioned at 3 nm intervals along the nanotube surface, provide unique hybrid nanostructures in which the photoinduced CS dynamics involving the (6,5) SWNT singlet excited state (^{1}[(6,5) SWNT]*) and the PDI electron-acceptor, as well as the corresponding thermal CR reaction dynamics involving the SWNT hole polaron state [(6,5) SWNT$^{(\bullet+)n}$] and the PDI radical anion (PDI$^{-\bullet}$), can be unambiguously characterized by pump–probe transient absorption spectroscopy.

Established GPC purification methods show that *S*-PBN(b)-Ph_4PDI-[(6,5) SWNT] superstructures feature no measurable concentration of uncomplexed *S*-PBN(b)-Ph_4PDI (Scheme 1; Supporting Information, Figure S4).[7,8c] Vis-NIR absorption spectra of *S*-PBN(b)-Ph_4PDI-[(6,5) SWNTs] and S-PBN(b)-Ph_5-[(6,5) SWNTs] are shown in the Supporting Information, Figure S8. Note that *S*-PBN(b)-Ph_5-[(6,5) SWNTs] feature a polymeric structure that has previously been established to act strictly as a nanotube solubilizing agent.[7] The spectral data in the Supporting Information Figure S8, indicate similar bathochromic shifts of the E_{11} (ca. 235 cm^{-1}) and E_{22} transitions (ca. 173 cm^{-1}) of water-suspended *S*-PBN(b)-Ph_4PDI-[(6,5) SWNTs] and *S*-PBN(b)-Ph_5-[(6,5) SWNTs] relative to the analogous transitions observed for benchmark sodium cholate (SC)-suspended [(6,5) SWNT] samples (SC-[(6,5) SWNTs]); previous work suggests that such modest SWNT E_{nn} spectral shifts derive in large part from differences in the extent to which polymer-wrapped nanotube samples are solvated relative to SC surfactant-dispersed SWNTs.[1a]

The potentiometric band gaps of the *S*-PBN(b)-Ph_4PDI-[(6,5) SWNT] and *S*-PBN(b)-Ph_5-[(6,5) SWNT] superstructures were determined by square-wave and cyclic voltammetry methods. Note that the initial oxidation and reduction potentials of *S*-PBN(b)-Ph_5-[(6,5) SWNTs] ($E^{0/+}=0.48$ V; $E^{-/0}=-1.10$ V vs. SCE; Supporting Information, Figure S8) are far removed from the corresponding values that define the potentiometrically determined HOMO–LUMO gap of the unbound anionic polymer S-PBN(b)-Ph_5 ($E^{0/+}=0.91$ V; $E^{-/0}=-1.62$ V vs. SCE): these $E^{0/+}=0.48$ V and $E^{-/0}=-1.10$ V redox values thus correspond to the electrode potentials at which holes and electrons are injected respectively into the (6,5) SWNT valence and conduction bands (Figure 1). In contrast, the *S*-PBN(b)-Ph_4PDI polymer manifests a first reduction potential at -0.53 V, followed by a second reduction potential at -0.70 V (Figure 1): these values match closely the previously reported $E^{-/0}$ and $E^{2-/-}$ potentials of water-soluble PDI derivatives.[12] While the reduction potential of the (6,5) SWNT component of the *S*-PBN(b)-Ph_4PDI-[(6,5) SWNT] superstructure has been raised by 0.15 V relative to that observed for the control sample (Figure 1; Supporting Information, Figure S11), note that the measured first and second reduction potentials of PDI moieties of *S*-PBN(b)-Ph_4PDI-[(6,5) SWNTs] shift

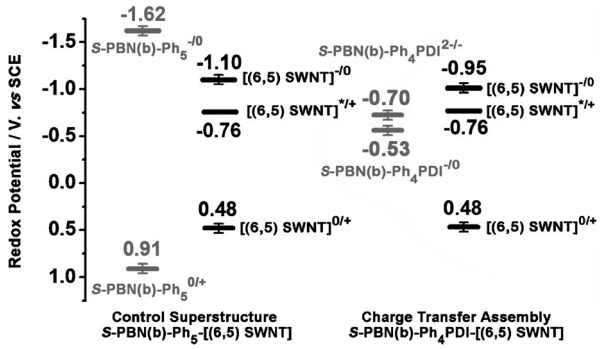

Figure 1. Energy level diagram highlighting the experimentally determined redox potentials of the polymer and SWNT components of *S*-PBN(b)-Ph_5-[(6,5) SWNT] and *S*-PBN(b)-Ph_4PDI-[(6,5) SWNT] superstructures. The [(6,5) SWNT]$^{*/+}$ excited-state reduction potential was determined from the (6,5) SWNT $E_{00}\rightarrow E_{11}$ optical band gap ($\Delta E_{11}=1.24$ eV) and its ground state oxidation potential ($E^{0/+}=0.48$ V). In the potentiometric experiments used to determine these redox potentials, the ferrocene/ferrocenium (Fc/Fc^+) redox couple ($E_{1/2}{}^{0/+}=0.48$ V vs. SCE) was used as an internal standard. Experimental conditions: CH_2Cl_2 solvent, 0.1 M nBu$_4$NPF$_6$, $T=20$°C. Tabulated potentiometric data are available in the Supporting Information.

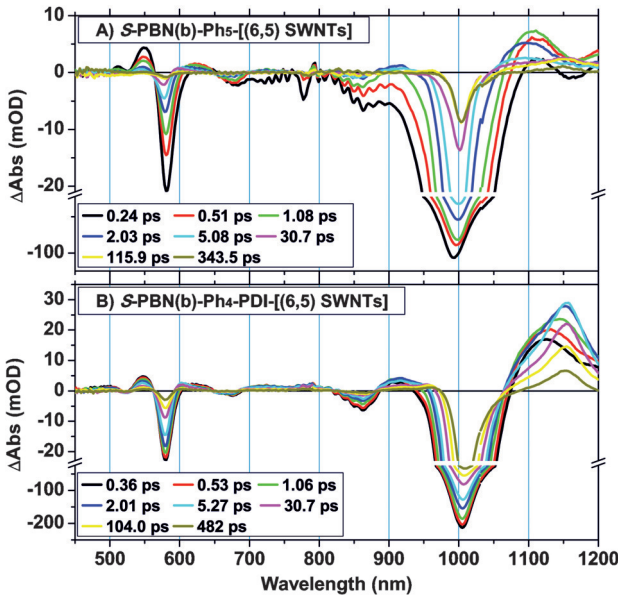

Figure 2. Representative transient absorption spectra recorded for A) *S*-PBN(b)-Ph_5-[(6,5) SWNT] and B) *S*-PBN(b)-Ph_4PDI-[(6,5) SWNT] samples dispersed in 3:7 MeOH/D_2O at the time delays noted. Experimental conditions: [(6,5) SWNTs] ca. 90.3 nM; SWNT length = 700 ± 50 nm; argon atmosphere; optical path length = 2 mm; $\lambda_{ex}=1000$ nm; pulse energy = 180 nJ/pulse; temperature = 20 °C; magic angle polarization.

cathodically by approximately 30 mV relative to the corresponding values determined for the PDI units in unbound S-PBN(b)-Ph_4PDI polymer (Figure 1). The Figure 1 energy level diagram summarizes the ground-state redox potentials for the polymeric and SWNT components of these *S*-PBN(b)-Ph_5-[(6,5) SWNT] and *S*-PBN(b)-Ph_4PDI-[(6,5) SWNT] superstructures, relative to the (6,5) SWNT excited state reduction potential ([(6,5) SWNTs]$^{*/+}=-0.76$ V vs. SCE). Based on the data in Figure 1, it is evident the ^{1}[(6,5) SWNT]* state generated via $E_{00}\rightarrow E_{11}$ photoexcitation ($\lambda_{ex}=1000$ nm) features neither an exergonic driving force for electron or energy transfer reaction with the polymer that wraps the surface of *S*-PBN(b)-Ph_5-[(6,5) SWNT] superstructures. In contrast, these data highlight that the ^{1}[(6,5) SWNT]* state possesses a significant driving force ($-\Delta G_{CS}=0.23$ V)[13] for electron injection into the n-type polymer LUMO of *S*-PBN(b)-Ph_4PDI-[(6,5) SWNT] hybrid assemblies. The notion that the ^{1}[(6,5) SWNT]* state possesses sufficient driving force to undergo a photoinduced electron transfer reaction within the *S*-PBN(b)-Ph_4PDI-[(6,5) SWNT] superstructure, but not within a *S*-PBN(b)-Ph_5-[(6,5) SWNT] construct, is borne out by steady-state fluorescence emission experiments, which highlight dramatic ^{1}[(6,5) SWNT]* fluorescence quenching in *S*-PBN(b)-Ph_4PDI-[(6,5) SWNTs] relative to the control *S*-PBN(b)-Ph_5-[(6,5) SWNT] sample (Supporting Information).

Figure 2 shows exemplary femtosecond (fs) pump–probe transient absorption spectroscopic data acquired for *S*-PBN(b)-Ph_5-[(6,5) SWNT] and *S*-PBN(b)-Ph_4PDI-[(6,5) SWNT] samples following $E_{00}\rightarrow E_{11}$ excitation over a 100 fs–2 ns time domain. In these experiments, *S*-PBN(b)-Ph_5-[(6,5) SWNT] and S-PBN(b)-Ph_4PDI-[(6,5) SWNT] samples were selectively excited at $\lambda_{ex}=1000$ nm; a white continuum probe beam was utilized, allowing spectral evolution to be monitored concomitantly over the Vis-NIR spectral range. Congruent with previous experiments,[6a,14] transient dynamical data obtained for *S*-PBN(b)-Ph_5-[(6,5) SWNTs] (Figure 2 A) display spectral features dominated by ground-state bleaching bands in both the E_{11} and E_{22} spectral regions. Note that over the 900–1250 nm spectral regime two transient absorptions at about 1100 and 1150 nm are also evident: these signals correspond respectively to exciton to biexciton ($E_{11}\rightarrow E_{11,BX}$)[9,15] and $T_1\rightarrow T_n$ ($^3E_{11}\rightarrow{}^3E_{nn}$)[6a,16] transitions.

Figure 2 B shows pump–probe transient dynamical data acquired for *S*-PBN(b)-Ph_4PDI-[(6,5) SWNTs]: along with the characteristic transient bleaching signals of [(6,5) SWNTs] highlighted in Figure 2 A, note the appearance of a new absorption feature at 1155 nm that emerges at $t_{delay}>\approx 0.5$ ps and is clearly evident at $t_{delay}=2$ ps for the *S*-PBN(b)-Ph_4PDI-[(6,5) SWNT] sample; this signal, and its spectral evolution, are distinct from that of the (6,5) SWNT $T_1\rightarrow T_n$ transition[6a] at 1150 nm (Figure 2 A). Furthermore, the transient absorption spectrum for *S*-PBN(b)-Ph_4PDI-[(6,5) SWNTs] at $t_{delay}=0.3$ ps exhibits a broad signal centered at about 1120 nm that rapidly decays over an approximate 5 ps time domain (Figure 2 B). In stark contrast, the NIR transient absorption spectra acquired for *S*-PBN(b)-Ph_5-[(6,5) SWNTs] over the initial 10 ps time window manifest spectral evolution characteristic of conventional, electronically excited [(6,5) SWNTs]:[6a] 1) the $E_{11}\rightarrow E_{11,BX}$ transition at 1100 nm is evident immediately following photoexcitation at $t_{delay}=300$ fs,[6c,15b,16] and 2) the $^3E_{11}\rightarrow{}^3E_{nn}$ signal at about 1150 nm appears at $t_{delay}>7$ ps, rises over an approximate 10–20 ps time window, and persists beyond the instrumental limit of 3 ns. The spectral and dynamical features observed near 1155 nm in the pump–probe transient absorption spectra

acquired for electronically excited *S*-PBN(b)-Ph_4PDI-[(6,5) SWNTs] indicate formation of a new absorptive species clearly distinct from the ^{3}[(6,5) SWNT]* state.

To gain further insight into the spectral signatures that should be associated with an oxidized (6,5) SWNT, an oxidative titration of a *S*-PBN(b)-Ph_5-[(6,5) SWNT][10,17] sample was carried out using a chemical oxidant (0.5 mM K_2IrCl_6 (+0.65 V vs. SCE in H_2O)) and monitored by steady-state electronic absorption spectroscopy (Supporting Information, Figure S14B). With increasing oxidant concentration, a progressive diminution of both $E_{00}\rightarrow E_{11}$ and $E_{00}\rightarrow E_{22}$ transition oscillator strength occurs, with concomitant rise of a new low energy transition centered at 1155 nm; this transition is thus assigned to an absorption associated with the (6,5) SWNT hole polaron state[18] [(6,5) SWNT$^{(\bullet+)n}$], congruent with earlier precedent.[10,17]

If formation of the [(6,5) SWNT$^{(\bullet+)n}$] state occurred by a photoinduced charge-separation reaction that followed electronic excitation *S*-PBN(b)-Ph_4PDI-[(6,5) SWNTs], the emergence of the characteristic PDI-derived polymer radical anion transient absorption signals must occur concomitantly. Figure 3 compares Vis-NIR transient absorption data

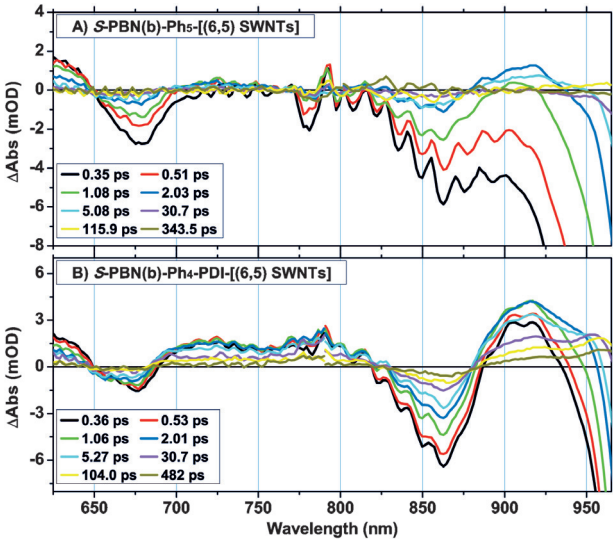

Figure 3. Comparative transient absorption spectra obtained for A) *S*-PBN(b)-Ph_5-[(6,5) SWNT] and B) *S*-PBN(b)-Ph_4PDI-[(6,5) SWNT] samples dispersed in 3:7 MeOH/D_2O at the time delays noted. Experimental conditions: [(6,5) SWNTs] ca. 90.3 nM; SWNT length = 700 ± 50 nm; argon atmosphere; optical path length = 2 mm; λ_{ex} = 1000 nm; pulse energy = 180 nJ/pulse; temperature = 20 °C; magic angle polarization.

obtained for *S*-PBN(b)-Ph_4PDI-[(6,5) SWNT] and *S*-PBN(b)-Ph_5-[(6,5) SWNT] samples dispersed in 3:7 MeOH/D_2O at time delays ranging from 0.3–500 ps over the 625–975 nm spectral domain. Note that spectra acquired for *S*-PBN(b)-Ph_4PDI-[(6,5) SWNTs] over $0 < t_{delay} < 100$ ps manifest critical features absent in spectra acquired over similar time delays for the control *S*-PBN(b)-Ph_5-[(6,5) SWNT] superstructure: transient signals evident over the 625–800 and 880–950 nm windows point to the formation of a new species following (6,5) SWNT photoexcitation in *S*-PBN(b)-Ph_4PDI-[(6,5) SWNT] samples. To confirm the nature of this new absorptive species, a reductive titration of the unbound anionic *S*-PBN(b)-Ph_4PDI polymer with sodium dithionate (−0.90 V vs. SCE) in 3:7 MeOH/D_2O was carried out (Supporting Information, Figure S14A). These reductive titration experiments evince the formation of new absorption bands centered at 755, 844, 902, and 1032 nm; these transitions correspond to the established ground-state spectral signatures of the PDI$^{-\bullet}$ radical anion.[11a,12a]

A similar reductive titration was carried out with a *S*-PBN(b)-Ph_4PDI-[(6,5) SWNT] sample; note that these same characteristic PDI$^{-\bullet}$ absorptions are evident (Supporting Information, Figure S14C). Unperturbed (6,5) SWNT $E_{00}\rightarrow E_{11}$ and $E_{00}\rightarrow E_{22}$ absorption bands highlighted in the data in the Supporting Information, Figure S13 are consistent with expectations based on the Figure 1 energy level diagram: the (6,5) SWNT reduction potential in *S*-PBN(b)-Ph_4PDI-[(6,5) SWNT] superstructures [$E^{-/0}$[(6,5) SWNTs] = −0.95 V vs. SCE] lies at lower potential than that of the n-type polymer ($E^{-/0}$(*S*-PBN(b)-Ph_4PDI) = −0.53 V vs. SCE). These reductive titration experiments (Supporting Information, Figure S14) demonstrate unambiguously that electronic excitation of *S*-PBN(b)-Ph_4PDI-[(6,5) SWNTs] generates the PDI radical anion[11a,b] by a photoinduced CS reaction (Figure 3A).

While redox titration data (Supporting Information, Figure S14) confirm the spectral signatures of the charge-separated [(6,5) SWNT$^{(\bullet+)n}$]-(PDI$^{-\bullet}$)$_n$ state evident in the pump–probe transient absorption spectral data acquired for *S*-PBN(b)-Ph_4PDI-[(6,5) SWNTs] (Figures 2 and 3), monitoring of the $E_{00}\rightarrow E_{11}$ ground-state bleaching signal as a function of delay time (Supporting Information, Figure S15) for *S*-PBN(b)-Ph_4PDI-[(6,5) SWNT], *S*-PBN(b)-Ph_5-[(6,5) SWNT], and SC-(6,5) SWNT samples, highlights that in contrast to electronically excited *S*-PBN(b)-Ph_5-[(6,5) SWNTs] and SC-(6,5) SWNTs, which exhibit ground-state recovery on a tens of ps timescale,[6a,14,19] photoexcitation of S-PBN(b)-Ph_4PDI-[(6,5) SWNTs] results in $E_{00}\rightarrow E_{11}$ bleaching band recovery dynamics that are significantly slower. Time constants for photoinduced charge separation (τ_{CS}) and thermal charge recombination (τ_{CR}) were determined from multiwavelength global analysis (Supporting Information, Figure S16); corresponding fitting results are displayed in the Supporting Information, Table S1. Monitoring the rise of the PDI ground-state bleach signal at λ_{pr} = 523.7 nm and the rise of transient absorptive signature of ET products ([(6,5) SWNT$^{(\bullet+)n}$] and PDI$^{-\bullet}$ determines $\tau_{CS} \approx 0.4$ ps (Φ_{CS} = 97 %). The decay dynamics of the [(6,5) SWNT$^{(\bullet+)n}$] and PDI$^{-\bullet}$ transient absorptive signature monitored at 754, 850, 950, and 1155 nm provide two charge recombination time constants ($\tau_{CR} \approx 31.8$ and 250 ps). The fact that the rise and decay kinetics of the [(6,5) SWNT$^{(\bullet+)n}$] and PDI$^{-\bullet}$ transient absorptive signals mirror each other solidify the photoinduced CS and thermal CR dynamical summary presented in Figure 4A. It is important to note that this result represents the first unambiguous diagnosis of photoinduced charge carrier generation at nanotube–soft-matter interfaces. Furthermore, the near unity quantum yield of charge separation (Φ_{CS} = 97 %) exhibited in *S*-PBN(b)-Ph_4PDI-[(6,5) SWNT] samples under

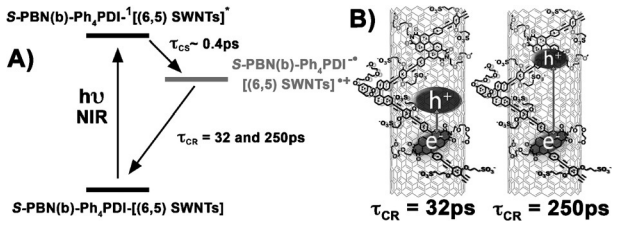

Figure 4. Representation of the A) photoinduced charge separation (CS) and thermal charge recombination (CR) dynamics observed following $E_{00} \rightarrow E_{11}$ excitation ($\lambda_{ex} = 1000$ nm) for the *S*-PBN(b)-Ph_4PDI-[(6,5) SWNT] nanoscale assembly and B) CR dynamics involving both an intimately associated SWNT hole polaron and $PDI^{-\bullet}$, and a related charge-separated state involving $PDI^{-\bullet}$ and a SWNT hole polaron derived from charge migration to an adjacent hole polaron site along the SWNT backbone.[20]

these excitation conditions (Supporting Information) underscores the utility of these compositions, which rigorously define electron donor and acceptor stoichiometry, for NIR photon capture and subsequent energy conversion; these systems thus stand in sharp contrast to the excited-state dynamics exhibited by heterogeneous SWNT–polymer blends, and highlight the potential for this class of structurally well-defined semiconducting polymer–carbon-nanotube superstructures as solar-cell materials.

With respect to the biphasic nature of the CR dynamics for *S*-PBN(b)-Ph_4PDI-[(6,5) SWNTs], it is important to note that the slower 250 ps component corresponds well with the τ_{CR} (ca. 300 ps) value reported by Hirsch and Guldi, who examined photoinduced electron-transfer reactions involving electronically excited heterogeneous SWNT samples and perylene dye-based surfactants.[5a] While the data presented herein cannot ascribe a precise origin for the two CR timescales, given the combination of large magnitude SWNT hole polaron migration rates[21] and the substantial hole polaron delocalization length (2.75 nm in (6,5) SWNTs),[10] these 31.8 and 250 ps τ_{CR} values for *S*-PBN(b)-Ph_4PDI-[(6,5) SWNTs] may reflect CR dynamics involving both an intimately associated SWNT hole polaron and $PDI^{-\bullet}$ charge-separated state, and a related charge-separated state involving $PDI^{-\bullet}$ and a hole polaron site produced via hole migration along the SWNT backbone that occurs over this timescale (Figure 4B).[22]

In summary, the *S*-PBN(b)-Ph_4PDI-[(6,5) SWNT] superstructure, in which a chiral [arylene]ethynylene polymer helically wraps the nanotube surface in an exclusive left-handed, single-chain fashion, defines the first example of a carbon-nanotube–soft-matter assembly that enables the electronic signatures that distinguish electron-transfer reactants and products, and corresponding analyses of charge separation (CS), charge migration, and charge recombination (CR) dynamics, to be readily elucidated. These SWNT-based nanohybrid compositions are based on (6,5) chirality-enriched SWNTs ([(6,5) SWNTs] and a chiral n-type polymer (*S*-PBN(b)-Ph_4PDI) that exploits a perylenediimide (PDI)-containing repeat unit; *S*-PBN(b)-Ph_4PDI-[(6,5) SWNT] superstructures feature a PDI electron acceptor unit positioned at 3 nm intervals along the nanotube surface, thus controlling rigorously SWNT/electron acceptor stoichiometry and organization. Time-resolved pump–probe spectroscopic studies demonstrate that *S*-PBN(b)-Ph_4PDI-[(6,5) SWNT] electronic excitation generates the PDI radical anion ($PDI^{-\bullet}$) via a photoinduced CS reaction ($\tau_{CS} \approx 0.4$ ps). These experiments highlight the concomitant rise and decay of transient absorption spectroscopic signatures characteristic of the SWNT hole polaron [(6,5) $SWNT^{(\bullet+)n}$] and $PDI^{-\bullet}$ states. Multiwavelength global analysis of these data provides two charge recombination time constants ($\tau_{CR} \approx 31.8$ and 250 ps). These two CR time constants likely reflect CR dynamics involving both an intimately associated SWNT hole polaron and $PDI^{-\bullet}$ charge-separated state, and a related charge-separated state involving $PDI^{-\bullet}$ and a hole polaron site produced via hole migration along the SWNT backbone that occurs over this timescale; this analysis mirrors dynamical descriptions of the photoinduced charge separation and thermal charge recombination dynamics involving semiconducting polymers in the solid state.[22] This work thus defines a viable strategy to control the stoichiometry of electron (hole) acceptors at the nanotube interface, regulate the hole (electron) polaron density generated per nanotube unit length for a defined set of irradiation conditions, and engineer nanotube–soft-matter assemblies in which critical energy transduction dynamical processes may be modulated.

Keywords: nanoscale assembly · photoinduced charge-transfer · redox-active polymers · semiconducting materials · single-walled nanotubes

How to cite: *Angew. Chem. Int. Ed.* **2015**, *54*, 8133–8138
Angew. Chem. **2015**, *127*, 8251–8256

[1] a) B. A. Larsen, P. Deria, J. M. Holt, I. N. Stanton, M. J. Heben, M. J. Therien, J. L. Blackburn, *J. Am. Chem. Soc.* **2012**, *134*, 12485–12491; b) P. J. F. Harris, *Carbon Nanotube Science* Cambridge, UK, **2009**; c) P. Avouris, M. Freitag, V. Perebeinos, *Nat. Photonics* **2008**, *2*, 341–350; d) M. J. O'Connell, S. M. Bachilo, C. B. Huffman, V. C. Moore, M. S. Strano, E. H. Haroz, K. L. Rialon, P. J. Boul, W. H. Noon, C. Kittrell, J. Ma, R. H. Hauge, R. B. Weisman, R. E. Smalley, *Science* **2002**, *297*, 593–596; e) S. M. Bachilo, M. S. Strano, C. Kittrell, R. H. Hauge, R. E. Smalley, R. B. Weisman, *Science* **2002**, *298*, 2361–2366; f) L. J. Carlson, T. D. Krauss, *Acc. Chem. Res.* **2008**, *41*, 235–243.

[2] a) Q. Cao, S.-j. Han, G. S. Tulevski, Y. Zhu, D. D. Lu, W. Haensch, *Nat. Nanotechnol.* **2013**, *8*, 180–186; b) P. Avouris, Z. Chen, V. Perebeinos, *Nat. Nanotechnol.* **2007**, *2*, 605–615; c) J. Hone, M. C. Llaguno, N. M. Nemes, A. T. Johnson, J. E. Fischer, D. A. Walters, M. J. Casavant, J. Schmidt, R. E. Smalley, *Appl. Phys. Lett.* **2000**, *77*, 666–668; d) S. J. Tans, A. R. M. Verschueren, C. Dekker, *Nature* **1998**, *393*, 49–52; e) M. Bockrath, D. H. Cobden, P. L. McEuen, N. G. Chopra, A. Zettl, A. Thess, R. E. Smalley, *Science* **1997**, *275*, 1922–1925; f) H. Dai, E. W. Wong, C. M. Lieber, *Science* **1996**, *272*, 523–526.

[3] a) D. J. Bindl, M. S. Arnold, *J. Phys. Chem. C* **2013**, *117*, 2390–2395; b) M. S. Arnold, J. L. Blackburn, J. J. Crochet, S. K. Doorn, J. G. Duque, A. Mohite, H. Telg, *Phys. Chem. Chem. Phys.* **2013**, *15*, 14896–14918.

[4] a) F. D'Souza, S. K. Das, M. E. Zandler, A. S. D. Sandanayaka, O. Ito, *J. Am. Chem. Soc.* **2011**, *133*, 19922–19930; b) C. Romero-Nieto, R. García, M. Á. Herranz, C. Ehli, M. Ruppert, A. Hirsch, D. M. Guldi, N. Martín, *J. Am. Chem. Soc.* **2012**, *134*, 9183–9192; c) F. G. Brunetti, C. Romero-Nieto, J. López-

Andarias, C. Atienza, J. L. López, D. M. Guldi, N. Martín, *Angew. Chem. Int. Ed.* **2013**, *52*, 2180 – 2184; *Angew. Chem.* **2013**, *125*, 2236 – 2240; d) Q. Zhong, V. V. Diev, S. T. Roberts, P. D. Antunez, R. L. Brutchey, S. E. Bradforth, M. E. Thompson, *ACS Nano* **2013**, *7*, 3466 – 3475.

[5] a) C. Ehli, C. Oelsner, D. M. Guldi, A. Mateo-Alonso, M. Prato, C. Schmidt, C. Backes, F. Hauke, A. Hirsch, *Nat. Chem.* **2009**, *1*, 243 – 249; b) U. Hahn, S. Engmann, C. Oelsner, C. Ehli, D. M. Guldi, T. Torres, *J. Am. Chem. Soc.* **2010**, *132*, 6392 – 6401; c) A. J. Hilmer, K. Tvrdy, J. Zhang, M. S. Strano, *J. Am. Chem. Soc.* **2013**, *135*, 11901 – 11910; d) C. Romero-Nieto, R. García, M. Á. Herranz, L. Rodríguez-Pérez, M. Sánchez-Navarro, J. Rojo, N. Martín, D. M. Guldi, *Angew. Chem. Int. Ed.* **2013**, *52*, 10216 – 10220; *Angew. Chem.* **2013**, *125*, 10406 – 10410; e) A. de Juan, Y. Pouillon, L. Ruiz-González, A. Torres-Pardo, S. Casado, N. Martín, Á. Rubio, E. M. Pérez, *Angew. Chem. Int. Ed.* **2014**, *53*, 5394 – 5400; *Angew. Chem.* **2014**, *126*, 5498 – 5504.

[6] a) J. Park, P. Deria, M. J. Therien, *J. Am. Chem. Soc.* **2011**, *133*, 17156 – 17159; b) M. S. Arnold, A. A. Green, J. F. Hulvat, S. I. Stupp, M. C. Hersam, *Nat. Nanotechnol.* **2006**, *1*, 60 – 65.

[7] P. Deria, C. D. Von Bargen, J.-H. Olivier, A. S. Kumbhar, J. G. Saven, M. J. Therien, *J. Am. Chem. Soc.* **2013**, *135*, 16220 – 16234.

[8] a) Y. K. Kang, O.-S. Lee, P. Deria, S. H. Kim, T.-H. Park, D. A. Bonnell, J. G. Saven, M. J. Therien, *Nano Lett.* **2009**, *9*, 1414 – 1418; b) P. Deria, L. E. Sinks, T.-H. Park, D. M. Tomezsko, M. J. Brukman, D. A. Bonnell, M. J. Therien, *Nano Lett.* **2010**, *10*, 4192 – 4199; c) J.-H. Olivier, P. Deria, J. Park, A. Kumbhar, M. Andrian-Albescu, M. J. Therien, *Angew. Chem. Int. Ed.* **2013**, *52*, 13080 – 13085; *Angew. Chem.* **2013**, *125*, 13318 – 13323.

[9] J. Park, P. Deria, J.-H. Olivier, M. J. Therien, *Nano Lett.* **2014**, *14*, 504 – 511.

[10] P. Deria, J.-H. Olivier, J. Park, M. J. Therien, *J. Am. Chem. Soc.* **2014**, *136*, 14193 – 14199.

[11] a) D. Gosztola, M. P. Niemczyk, W. Svec, A. S. Lukas, M. R. Wasielewski, *J. Phys. Chem. A* **2000**, *104*, 6545 – 6551; b) W. E. Ford, H. Hiratsuka, P. V. Kamat, *J. Phys. Chem.* **1989**, *93*, 6692 – 6696; c) T. van der Boom, R. T. Hayes, Y. Zhao, P. J. Bushard, E. A. Weiss, M. R. Wasielewski, *J. Am. Chem. Soc.* **2002**, *124*, 9582 – 9590; d) M. T. Vagnini, A. L. Smeigh, J. D. Blakemore, S. W. Eaton, N. D. Schley, F. D′Souza, R. H. Crabtree, G. W. Brudvig, D. T. Co, M. R. Wasielewski, *Proc. Natl. Acad. Sci. USA* **2012**, *109*, 15651 – 15656; e) L. F. Dössel, V. Kamm, I. A. Howard, F. Laquai, W. Pisula, X. Feng, C. Li, M. Takase, T. Kudernac, S. De Feyter, K. Müllen, *J. Am. Chem. Soc.* **2012**, *134*, 5876 – 5886.

[12] a) R. O. Marcon, S. Brochsztain, *J. Phys. Chem. A* **2009**, *113*, 1747 – 1752; b) E. Shirman, A. Ustinov, N. Ben-Shitrit, H. Weissman, M. A. Iron, R. Cohen, B. Rybtchinski, *J. Phys. Chem. B* **2008**, *112*, 8855 – 8858.

[13] The Gibbs energy for charge separation (ΔG_{CS}) was estimated using the equations $-(\Delta G_{CS}) = [E(0,0)\ (6,5)\ \text{SWNTs}] - [E^{0/+}\ (6,5)\ \text{SWNTs}]^{+}\ [E^{-/0}\ \text{S-PBN(b)-Ph}_4\text{PDI}]$, where E(0,0) is the energy of the first optically allowed transition E_{11} (6,5) SWNTs] (1.24 eV), $[E^{0/+}$ (6,5) SWNTs] is the onset potential for 6,5 SWNT valence band oxidation (0.48 V vs. SCE), and $[E^{-/0}$ S-PBN(b)-Ph_4PDI] is the electron reduction potential of the PDI-based polymer (−0.55 V vs SCE).

[14] a) Z. Zhu, J. Crochet, M. S. Arnold, M. C. Hersam, H. Ulbricht, D. Resasco, T. Hertel, *J. Phys. Chem. C* **2007**, *111*, 3831 – 3835; b) L. Lüer, S. Hoseinkhani, D. Polli, J. Crochet, T. Hertel, G. Lanzani, *Nat. Phys.* **2009**, *5*, 54 – 58.

[15] a) T. G. Pedersen, K. Pedersen, H. D. Cornean, P. Duclos, *Nano Lett.* **2005**, *5*, 291 – 294; b) D. J. Styers-Barnett, S. P. Ellison, B. P. Mehl, B. C. Westlake, R. L. House, C. Park, K. E. Wise, J. M. Papanikolas, *J. Phys. Chem. C* **2008**, *112*, 4507 – 4516.

[16] D. Stich, F. Späth, H. Kraus, A. Sperlich, V. Dyakonov, T. Hertel, *Nat. Photonics* **2014**, *8*, 138 – 144.

[17] M. Zheng, B. A. Diner, *J. Am. Chem. Soc.* **2004**, *126*, 15490 – 15494.

[18] Earlier work has ascribed this long wavelength transient absorptive spectral feature to an $E_{00} \rightarrow E_{trion}$ transition; see: R. Matsunaga, K. Matsuda, Y. Kanemitsu, *Phys. Rev. Lett.* **2011**, *106*, 037404; and S. Mouri, K. Matsuda, *J. Appl. Phys.* **2012**, *111*, 094309.

[19] a) Y. Z. Ma, L. Valkunas, S. L. Dexheimer, G. R. Fleming, *Mol. Phys.* **2006**, *104*, 1179 – 1189; b) M. S. Arnold, M. O. Guler, M. C. Hersam, S. I. Stupp, *Langmuir* **2005**, *21*, 4705 – 4709.

[20] Redox titration data indicate that a hole polaron site may be supported for each 2.75 nm of nanotube length; see Ref. [10].

[21] a) G. J. Brady, Y. Joo, S. Singha Roy, P. Gopalan, M. S. Arnold, *Appl. Phys. Lett.* **2014**, *104*, 083107; b) Q. Cao, S.-J. Han, G. S. Tulevski, A. D. Franklin, W. Haensch, *ACS Nano* **2012**, *6*, 6471 – 6477; c) R. Martel, T. Schmidt, H. R. Shea, T. Hertel, P. Avouris, *Appl. Phys. Lett.* **1998**, *73*, 2447 – 2449.

[22] Related dynamics observed in multi-polymer and polythiophene-PCBM blends have been ascribed to analogous geminate and non-geminate e-/h+ recombination reactions. See, for example: a) F. Etzold, I. A. Howard, N. Forler, D. M. Cho, M. Meister, H. Mangold, J. Shu, M. R. Hansen, K. Müllen, F. Laquai, *J. Am. Chem. Soc.* **2012**, *134*, 10569 – 10583; b) I. A. Howard, F. Laquai, P. E. Keivanidis, R. H. Friend, N. C. Greenham, *J. Phys. Chem. C* **2009**, *113*, 21225 – 21232; c) I. A. Howard, R. Mauer, M. Meister, F. Laquai, *J. Am. Chem. Soc.* **2010**, *132*, 14866 – 14876.

Received: February 11, 2015
Published online: May 26, 2015

